Self-Assembly of Gold Nanoparticles at the Surface of Amine- and Thiol-Functionalized Boron Nitride Nanotubes

Toby Sainsbury,[†,‡] Takashi Ikuno,[†,‡] David Okawa,[§] Daniela Pacilé,[‡] Jean M. J. Fréchet,[§,†] and Alex Zettl*[,†,‡]

Materials Sciences Division, Lawrence Berkeley National Laboratory, Department of Physics, and Department of Chemistry, University of California at Berkeley, Berkeley, California 94720

Received: April 16, 2007; In Final Form: May 23, 2007

Gold nanoparticles have been self-assembled at the surface of both amine- and thiol-functionalized boron nitride nanotubes (BNNTs) in solution. The chemical functionalization of the surface of the BNNTs was achieved following ammonia plasma irradiation in order to generate amine functional groups at the surface of the BNNTs. The amine-functionalized BNNTs (AF-BNNTs) were then covalently modified by the coupling of short-chain thiol-terminated organic molecules to result in thiol-functionalized BNNTs. The functionalization of the BNNTs was characterized using XPS, FT-IR spectroscopy, and EDS, whereas the nanoparticle−nanotube assemblies were characterized using HR-TEM and EELS. This approach constitutes a basis for the preparation of highly functionalized BNNTs and their utilization as nanoscale templates for assembly and integration with other nanoscale materials.

Introduction

In recent years, considerable research effort has been directed toward the synthesis and characterization of nanoscale materials on account of their novel mechanical, electronic, thermal, and chemical properties.[1] In particular, nanotubes of both carbon and boron nitride have generated interest because of their remarkable intrinsic properties and their use in a range of technological applications.[2,3] A key feature that has enabled many of the developments concerning carbon nanotubes (CNTs) has been the ability for the surface of the nanotubes to be chemically modified or functionalized.[4] This has allowed the solubilization of CNTs in a range of solvents,[5] the integration with host materials to form composites,[6,7] and their assembly with other nanoscale materials in solution and at substrates.[8,9] These advancements in turn have allowed the utilization of CNT-based materials for the development of novel sensory, electronic, catalytic, and materials applications.[10−13]

Although there have been significant developments concerning CNTs, there has been comparatively little progress concerning boron nitride nanotubes (BNNTs) and their integration with nanoscale materials. Several reports in recent years have described the surface modification of BNNTs as a means by which BNNTs may be solubilized, their electronic properties modified, and also to template the immobilization of materials from solution.[14−20] Although these reports describe the utilization of BNNTs to integrate with materials such as polymers and biomolecules, the density of functional groups that facilitate such interactions at the surface of the BNNTs is believed to be low in comparison with the modification of CNTs or the surface modification of conventional condensed phase materials such as nanoparticles or nanorods. In this context, the modification of BNNTs, which results in the generation of high densities of functional groups at the surface of BNNTs, is believed to have much potential for the utilization of these materials as nanoscale templates and for the integration with other nanoscale materials to form assemblies for chemical and biochemical applications, electronic device components, or composite materials. One strategy that has been used to assemble and organize nanoscale materials is directed-self-assembly using specific functional groups.[21,22] In view of this, the surface functionalization of nanoscale materials is of much interest in order to control their assembly in solution and at substrates.

SCHEME 1: Self-Assembly of Gold Nanoparticles at the Surface of (a) an Amine-Functionalized BNNT and (b) a Thiol-Functionalized BNNT

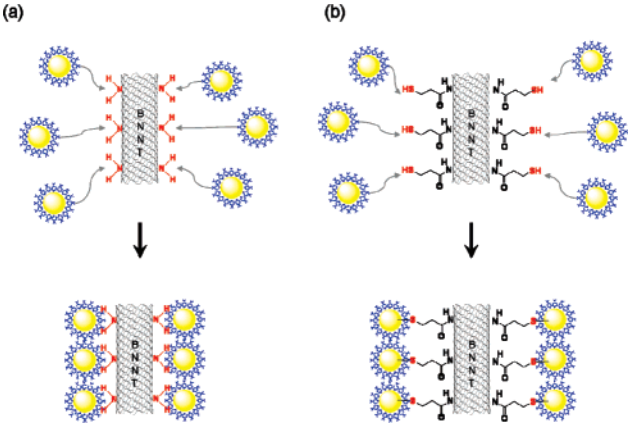

Recently, we have described the preparation of amine-functionalized BNNTs (AF-BNNTs).[23] Here we utilize the ability to generate amine functional groups at the surface of BNNTs by covalently modifying BNNTs with short-chain organic molecules that are terminated by thiol functional groups. Both the amine- and thiol-functionalized BNNTs were then used to direct the covalent self-assembly of gold nanoparticles in solution as illustrated in Scheme 1.

It is noted that using this covalent approach toward the directed self-assembly of gold nanoparticles from solution results in dense monolayer coverage of the particles on the BNNTs in

* Corresponding author. E-mail: azettl@berkeley.edu. Tel: 510-642-4939. Fax: 510-643-8793.
[†] Materials Sciences Division.
[‡] Department of Physics.
[§] Department of Chemistry.

10.1021/jp072958n CCC: $37.00
Published on Web 07/24/2007

both cases. The interaction between the gold nanoparticles and the BNNTs is mediated by a weak covalent bond in the case of the amine-functionalized BNNTs and a strong covalent bond in the case of the thiol-functionalized BNNTs. This allows the immobilization of dense networks of gold nanoparticles on BNNTs, which is of interest for the controlled assembly of nanoscale architectures and devices based on such materials.

Experimental Section

All solvents and compounds were used as supplied by the Sigma-Aldrich Chemical Co. Inc., unless otherwise stated.

XPS measurements were performed at the Molecular Foundry division of Lawrence Berkeley National Laboratory (LBNL) using an ultrahigh vacuum (UHV) chamber with a base pressure below 5×10^{-9} Torr. XPS data was collected using an X-ray photoelectron spectrometer PHI 5400 (Physical Electronics) with a nominal energy resolution of 0.7 eV. Spectra were acquired using a photon beam of 1486.6 eV, selected from a conventional (nonmonochromatic) Al/Mg dual-anode X-ray source. Data was collected at room temperature, and samples were analyzed as prepared, without any extra cleaning procedure under vacuum, to avoid possible desorption of molecular species from AF-BNNTs. The binding energies were corrected for specimen charging by referencing the C1s peak to 284.6 eV. The contamination level (O and C) was found to be very similar for pristine and amine-functionalized samples and within an acceptable limit (below 10%), as obtained from wide XPS spectra (not shown) and was estimated by taking into account the area of each peak with respect to the background and the cross section for the energies involved.

FT-IR spectroscopy was performed using a Mattson Infinity FT-IR spectrometer. Spectra of BNNTs and molecules were obtained using KBr pellets (0.05 mg in 100.00 mg of KBr). EDS analysis of BNNTs samples was performed using a FEI Sirion Field Emission SEM operated at 30 keV.

HR-TEM was performed using a JEOL 2010 (at an accelerating voltage of 200 kV) and a Philips CM-200 (at an accelerating voltage of 200 kV). The preparation of samples for TEM analysis involved depositing a drop (20 μL) of the relevant dispersion or suspension onto carbon-coated or 2000 square mesh copper TEM grids. EELS was performed using a Gatan 766 with the Philips CM-200. The elemental mapping acquisitions were performed using a three-window procedure. The slit width was 20 eV.

Preparation of BNNTs. BNNTs were synthesized according to a previously reported procedure.[24]

Preparation of Amine-Functionalized BNNTs (AF-BNNTs). Amine-functionalized BNNTs (AF-BNNTs) were prepared as described in detail elsewhere.[23]

Preparation of Mercaptopropionic Acid-Modified BNNTs (MPA-BNNTs). A solution of 3-mercaptopropionic acid (MPA) (50 μL, 5.74×10^{-4} mol), *N*-(3-dimethylaminopropyl)-*N*-ethylcarbodiimide hydrochloride (EDC) (0.132 g, 6.88×10^{-4} mol) and 4-dimethylaminopyridine (DMAP) (4.20×10^{-3} g, 3.44×10^{-5} mol) in deionized water (5 mL) was added to a freshly sonicated suspension of amine-functionalized BNNTs (0.5×10^{-3} gmL^{-1}) in deionized water (5 mL) and was allowed to stir for 12 h. The material was filtered using a membrane filtration apparatus (Cyclopore (0.2 μm pore diameter), Whatman), and washed with deionized water (1 L). The BNNT material was then sonicated off the filter membrane into deionized water (500 mL) and sonicated (5 min) in order to disperse the nanotubes. The material was filtered and washed once more using the membrane filtration apparatus in order to rid the BNNT material of any molecular contaminants. The MPA-modified BNNTs were then sonicated off the membrane filter into deionized water (10 mL).

Preparation of Butyryl Chloride-Modified BNNTs (BC-BNNTs) (Control Experiment). Butyryl Chloride (200 μL, 1.93×10^{-3} mol) was added to a freshly sonicated suspension of amine-functionalized BNNTs (0.5×10^{-3} gmL^{-1}) and pyridine (anhydrous)(40 μL, 4.95×10^{-4} mol) in dichloromethane (anhydrous)(5 mL), and was allowed to stir for 12 h. The material was filtered using a membrane filtration apparatus (Anodisc (0.02 μm pore diameter), Whatman), and washed with dichloromethane (500 mL). The BNNT material was then sonicated off the filter membrane into dichloromethane (500 mL) and sonicated (5 min) in order to disperse the nanotubes. The material was filtered and washed once more using the membrane filtration apparatus in order to rid the BNNT material of any molecular contaminants. The BC-modified BNNTs were then sonicated off the membrane filter into deionized water (10 mL). BC-modified BNNTs were characterized by FT-IR spectroscopy (see the Supporting Information).

Preparation of DMAP-Stabilized Gold Nanoparticles. DMAP-stabilized gold nanoparticles were prepared based on a procedure first reported by Caruso et al.[25] Briefly, this involved the reduction of an aqueous solution of gold salt in the presence of DMAP as follows: hydrogen tetrachloroaurate (III) trihydrate, (0.150 g, 0.380 mmol) was dissolved in deionized water (12 mL), resulting in a bright yellow solution. 4-Dimethylaminopyridine (DMAP) (0.250 g, 2.046 mmol) in chloroform (12 mL) was then added slowly to the vigorously stirring gold solution. Following the addition of the DMAP, the mixture turned a brown color ,which turns to bright orange after approximately 20 min of stirring. Vigorous stirring was continued for 2 h after which time the phases were separated, with the bright orange aqueous phase being retained. The bright-orange aqueous phase was then reduced by the addition of an aliquot (500 μL, 132 μmol) of a solution of sodium borohydride (0.100 g, 2.64 mmol) in deionized water (10 mL). The vigorously stirring solution was reduced instantaneously, producing a ruby-red dispersion of DMAP-stabilized gold nanoparticles. This dispersion was stirred for another hour and then filtered using membrane filtration apparatus (Millipore) in conjunction with a polycarbonate membrane filter (Whatman, Cyclopore, 20 nm pore diameter) in order to remove any aggregated material. The dispersion was characterized by TEM following dilution by deionized water (1:10) and evaporation of a drop (20 μL) onto a carbon-coated copper TEM grid.

Amine- and MPA-Modified BNNT Templated Self-Assembly of DMAP-Stabilized Gold Nanoparticles. DMAP-stabilized gold nanoparticles (40 μL, 26.3×10^{-3} gmL^{-1}) were added to a freshly sonicated (3 min) suspension of either amine-BNNTs or MPA-BNNTs (200 μL, 0.5×10^{-3} gmL^{-1}) in deionized water (800 μL) and were allowed to equilibrate for 12 h. A sample of the material was taken in the form of a precipitate that had formed at the bottom of the glass vial and was deposited onto a 2000 square mesh copper TEM grid for analysis.

As-Produced BNNTs with DMAP-Stabilized Gold Nanoparticles (Control Experiment). DMAP-stabilized gold nanoparticles (40 μL, 26.3×10^{-3} gmL^{-1}) were added to a freshly sonicated (3 min) suspension of as-produced BNNTs (200 μL, 0.5×10^{-3} gmL^{-1})) in deionized water (800 μL) and were allowed to equilibrate for 12 h. A sample of the material was taken in the form of a precipitate that had formed at the bottom

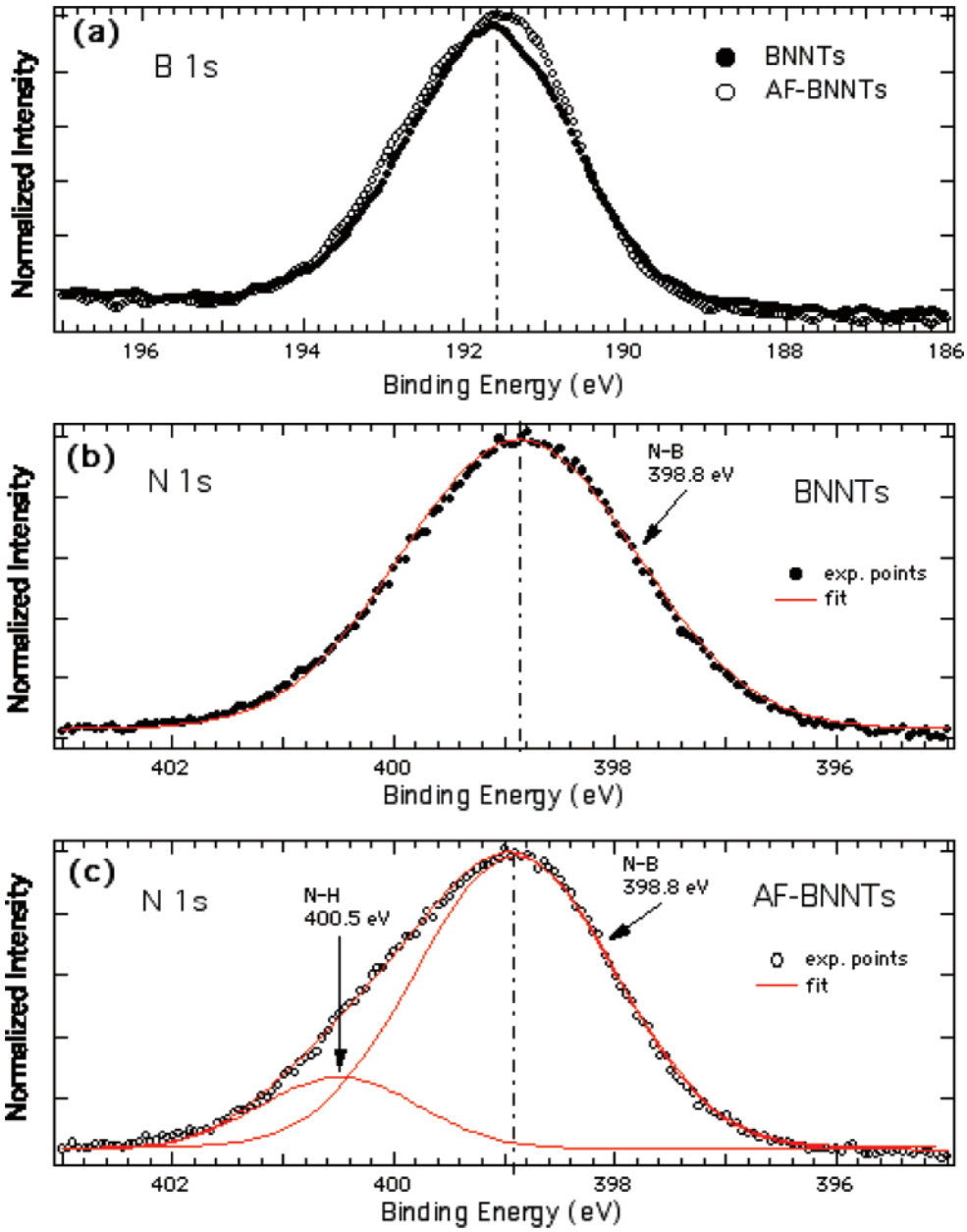

Figure 1. (a) B1s XPS spectrum of pristine BNNTs (full circles) and AF-BNNTs (empty circles). (b) N 1s XPS spectrum of pristine BNNTs (full circles) and its Gaussian component as obtained from the fit procedure (red solid line). (c) N 1s XPS spectrum of AF-BNNTs (empty circles) and its Gaussian components and sum (red solid lines).

of the glass vial and was deposited onto a carbon-coated copper TEM grid for analysis.

BC-Modified BNNTs with DMAP-Stabilized Gold Nanoparticles (Control Experiment). DMAP-stabilized gold nanoparticles (40 μL, 26.3×10^{-3} gmL^{-1}) were added to a freshly sonicated (3 min) suspension of BC-modified BNNTs (200 μL, 0.5×10^{-3} gmL^{-1})) in deionized water (800 μL) and were allowed to equilibrate for 12 h. A sample of the material was taken in the form of a precipitate that had formed at the bottom of the glass vial and was deposited onto a carbon-coated copper TEM grid for analysis.

Results and Discussion

For this study, BNNTs were synthesized using a CVD method and were subsequently exposed to an ammonia plasma in order to generate amine functional groups at the surface of the nanotubes, as described in detail elsewhere.[24,23]

Characterization of the amine groups at the surface of the BNNTs was achieved using X-ray photoelectron spectroscopy (XPS). Figure 1 shows XPS results obtained for as-prepared pristine BNNTs and AF-BNNTs.

Figure 1a shows a direct comparison between the B1s peaks for the two samples to highlight the similarity between our experimental results. Within our energy resolution the two peaks appear similar, both symmetric with respect to their center and with their maximum (corrected for the charging effect) located at approximately 191.5 eV, as expected from previous photoemission investigations.[26−28] Other possible components below the main peak, due to B−O and B−C bonds, are not resolved in our spectra, but they are expected to affect the B1s peak of the two samples in a similar way, although slight differences can justify some shoulders on the right and left side of the main components.

Analysis of the N1s peak (Figure 1b and c) indicates significant differences between the two samples. The N1s peak

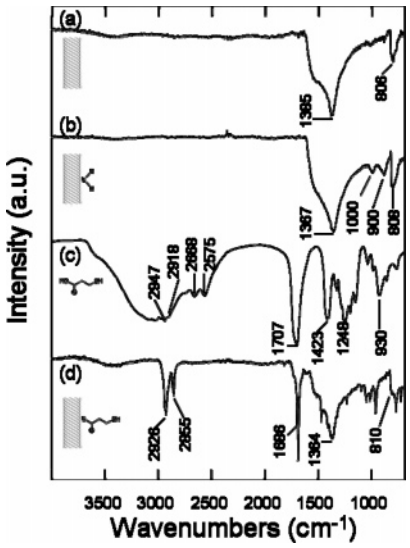

Figure 2. FT-IR spectra for (a) as-produced-BNNTs, (b) amine-modified BNNTs, (c) free 3-mercaptopropionic acid (MPA), and for (d) MPA-modified BNNTs.

SCHEME 2: Modification of Amine-Modified BNNTs with 3-Mercaptopropionic Acid (MPA) via Amide Formation

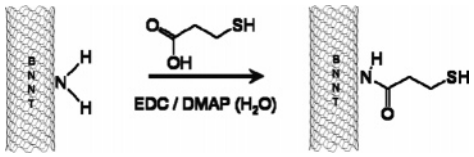

of pristine BNNTs (Figure 1b) is symmetric with respect to its center, and the fit procedure employs only the main Gaussian component, located at binding energy of 398.8 eV, as expected for N−B bonds.[26−28]

Alternatively, the N1s peak for the AF sample looks strongly asymmetric toward higher binding energies, and a second Gaussian component is found at 400.5 eV, as reported for N−H bonds on amine functionalized CNTs.[29] We can certainly rule out that this component is due to contaminants at the surface of AF-BNNTs because the N−O and N−C binding energies are expected at 401.5 and 398.6 eV, respectively.[30] Moreover, chemical shifts due to contaminants at surface (O and C) should affect the N1s peak of both pristine and doped samples in a similar way, as we found for the B1s peak (Figure 1a). The new component gives clear evidence of amine groups at the surface of AF-BNNTs, strongly suggesting that after the ammonia plasma treatment either H* or NH_2* radicals terminate some vacancies created at walls of BN tubes at either nitrogen or boron atoms, respectively.

The amine functional groups were then used to couple a short-chain organic molecule terminated with a thiol, 3-mercapto-propionic acid (MPA), to the surface of the BNNTs via standard diimide-mediated amide formation as illustrated in Scheme 2.

FT-IR spectroscopy was used to confirm the modification of the BNNTs with the short-chain MPA molecules. The spectrum of as-produced BNNTs (Figure 2a) exhibits two characteristic vibrational modes of BNNTs;[15−17,19,31−33] namely, the in-plane axial B−N−B vibration of the nanotubes, centered at 1385 cm^{-1} and the out-of-plane B−N vibration tangential to the nanotube axis, centered at 806 cm^{-1}. The spectrum of the amine-functionalized BNNTs (Figure 2b) exhibits a spectrum similar to that of the as-produced BNNTs; however, the heterogeneous environment of the surface-bound functional groups coupled with the large number of nanotube walls, which dominate the IR spectra, make identification of surface-bound amine groups nontrivial. The axial and tangential B−N vibrations appear at 1367 and 808 cm^{-1} respectively. The shift from 1385 to 1367 cm^{-1} for the axial vibration of the BNNTs is believed to be a consequence of the increased atomic disorder within the nanotubes following the amine functionalization of the BNNTs. Analogous broadening of these axial vibrations has also been noted previously by other authors.[17,32] The appearance of two vibrational modes at 1000 and 900 cm^{-1} are assigned to N−H out-of-plane bending absorptions of the amino groups and is also consistent with amine functionalization.

The spectrum of the free MPA molecule (Figure 2c) exhibits peaks in agreement with available reference spectra of the molecule.[34] The broad O−H stretch is identified between 3300 and 2500 cm^{-1}. The C−H stretching vibrations at 2947 cm^{-1} and a shoulder at 2927 cm^{-1} are superimposed upon the O−H stretch. The S−H of the thiol is identified as two peaks at 2668 and 2575 cm^{-1} on account of hydrogen bonding between the acid and thiol groups. The carboxylic C═O stretch is evident at 1707 cm^{-1}, whereas the C−O−H in plane bend and the C−O stretch are identified at 1423 and 1248 cm^{-1} respectively and the O−H out of plane bend at 930 cm^{-1}.

The FT-IR spectrum of the MPA-modified BNNTs (MPA-BNNTs) (Figure 2d) displays the characteristic vibrational modes of BNNTs at 1364 and 810 cm^{-1}. The appearance of peaks at 2926 and 2855 cm^{-1} are attributed to the asymmetric and symmetric C−H stretch of the methylene groups of the MPA molecules. The appearance of an intense peak centered at 1686 cm^{-1} is attributed to the C═O of the amide between the MPA molecules and the BNNT-amino groups. The shift of 21 cm^{-1} from the C═O of the free MPA acid provides strong support for the formation of the amide. Notably, the broad O−H band in the spectrum of the free MPA molecule has disappeared while the characteristic alkyl stretching vibrations have appeared in the spectrum of the MPA-BNNTs. The disappearance of prominent S−H stretching in the spectrum of the MPA-BNNTs (Figure 2d) coupled with the existence of the methylene stretching gives good evidence that the molecules are bound to the BNNTs and cannot intermolecularly hydrogen bond as seen in the spectrum of the free MPA molecule (Figure 2c). From the evidence presented in the spectrum of the MPA-BNNTs, it is concluded that the MPA is covalently bound to the surface of the BNNTs via amide formation.

Energy-dispersive X-ray spectroscopy (EDS) was used as an additional means to confirm the presence of the MPA molecules at the surface of the BNNTs. The EDS spectrum of the MPA-BNNTs shown in Figure 3 indicates the presence of B and N from the BNNTs and also C, O, and S from the MPA molecules. Peaks due to Mg and O are present because of the MgO material necessary for the synthesis of the BNNTs.[24]

The large sulfur peak evident in the EDS spectrum confirms that a significant amount of the MPA molecule is present at the surface of the BNNTs. Because of the intensive washing procedure of the materials following the coupling of the MPA molecules and the analysis by FT-IR, we conclude that there are essentially no residual free MPA molecules present and that all MPA present is covalently bound to the BNNTs. On this basis, we also conclude that the surfaces of the BNNTs are significantly functionalized with amino groups, which facilitate the covalent coupling of the MPA molecules. Although the specific binding of the amine groups to the sidewalls of the nanotubes is unclear at this point, we speculate that the binding of the amino groups to the B or N atoms occurs at a density

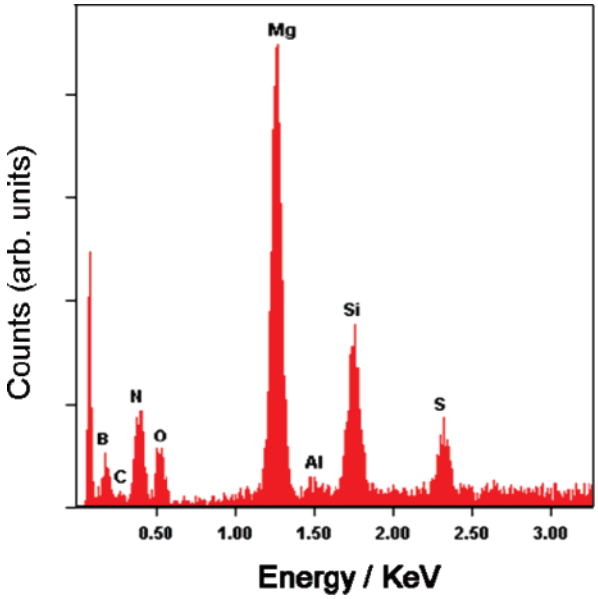

Figure 3. EDS spectrum of MPA-modified BNNTs indicating the presence of S from the MPA molecules.

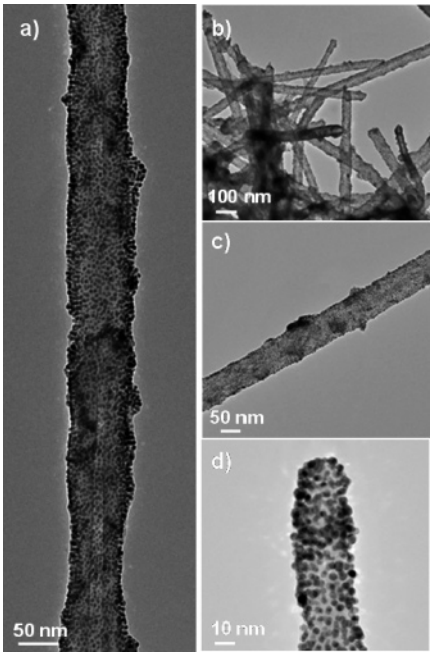

Figure 4. Typical low-resolution TEM images of DMAP-stabilized gold nanoparticles self-assembled at the surface of different amine-functionalized BNNTs, where the lengths of the BNNTs shown are approximately 750 nm (a), 1 μm (b), 600 nm (c), and 100 nm (d).

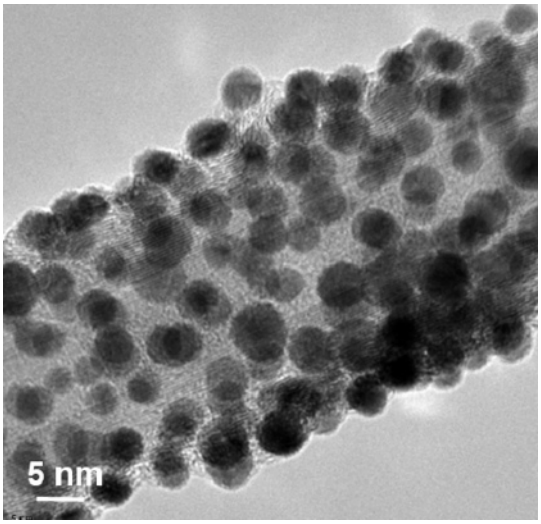

Figure 5. HR-TEM image of DMAP−Au nanoparticles self-assembled at the surface of an amine-functionalized BNNT.

such that the nanotubes retain their basic structural integrity despite the fact that bonds in the BNNTs lattice must be broken to accommodate either H* or NH_2* species, adding to either nitrogen or boron atoms in the lattice, respectively.[23] From the spectroscopic analysis of the modified BNNTs in this study, we can, however, conclude that significant modification of the BNNTs occurs using standard solution-based chemistry.

Aqueous dispersions of DMAP-stabilized gold nanoparticles were characterized using HR-TEM. The average particle diameter was determined to be 5 ± 0.5 nm from the analysis of 200 particles. The characteristic surface plasmon resonance maximum for the particles was observed at 518 nm (see the Supporting Information). The self-assembly of the gold nanoparticles at the surface of both the amine-modified and MPA-modified BNNTs involved the combination of aqueous suspensions of the materials. Following equilibration of the materials for 12 h, low-resolution and high-resolution TEM were used to characterize the BNNTs in both cases.

Figure 4 shows the amine-functionalized BNNTs covered in a monolayer of DMAP−Au nanoparticles following their combination in solution. The driving force for the interaction is believed to be the formation of a weak covalent bond between the BNNT bound amine functional groups and the surface of the gold nanoparticles. This type of interaction is common and has been exploited for the preparation of amine-stabilized gold nanoparticles and also for the immobilization of gold nanoparticles at the surface of carbon nanotubes and at substrates.[35−37] The images shown are representative of the sample and indicate that the BNNTs may be found as individual nanotubes, assembles, or aggregates of multiple nanotubes on the TEM grid.

High-resolution TEM (HR-TEM) was also used to characterize the self-assembly of the DMAP−Au nanoparticles at the surface of the amine-functionalized BNNTs (Figure 5). The average diameter and number density of the particles on the BNNT surface are roughly estimated to be 5 nm and 4.5 × 10^{12} cm^{-2}, respectively. The spacing between the particles ranges from 1 to 4 nm.

Figure 6 shows the results of the self-assembly of a monolayer of the DMAP-stabilized gold nanoparticles at the surface of the MPA-BNNTs. The nanoparticles were observed to form densely packed sheaths around the core of the BNNTs, as is evident in Figure 6c. The driving force for the interaction is covalent bond formation between the thiol groups on the BNNTs and the surface of the gold nanoparticles. The interaction between the thiol groups and the surface of the gold nanoparticles is believed to be possible because of the relative lability of the DMAP molecules. This allows the thiol groups to preferentially adsorb at the surface of the particles and thus facilitate assembly of the materials while forming a strong covalent S−Au bond. Similar examples of such interactions have also been demonstrated at the surface of thiol-modified CNTs.[38−40] Figure 6d shows a TEM image of a BNNT that is half-coated by a sheath of gold nanoparticles. Such structures appear occasionally and are postulated to occur as a result of a shadowing effect during the amine-functionalization of the BNNTs. Nanotubes that are shadowed by others might be expected to be unmodified by the process and as a result would not facilitate the assembly of

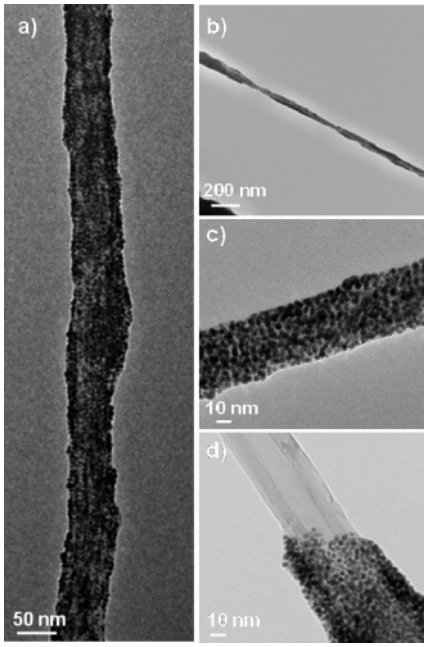

Figure 6. Typical low-resolution TEM images of DMAP-stabilized gold nanoparticles self-assembled at the surface of different MPA-modified BNNTs, where the lengths of the BNNTs shown are approximately 750 nm (a), 2 μm (b), 160 nm (c), and 180 nm (d).

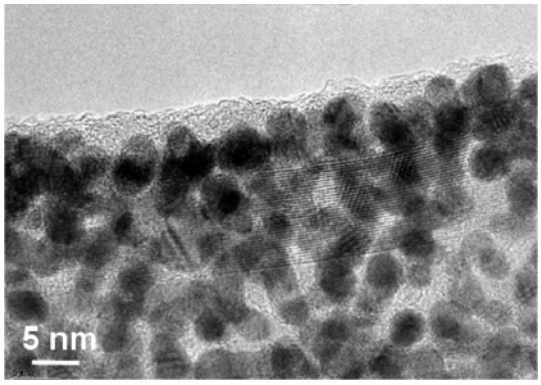

Figure 7. HR-TEM image of DMAP−Au nanoparticles self-assembled at the surface of an MPA-modified BNNT.

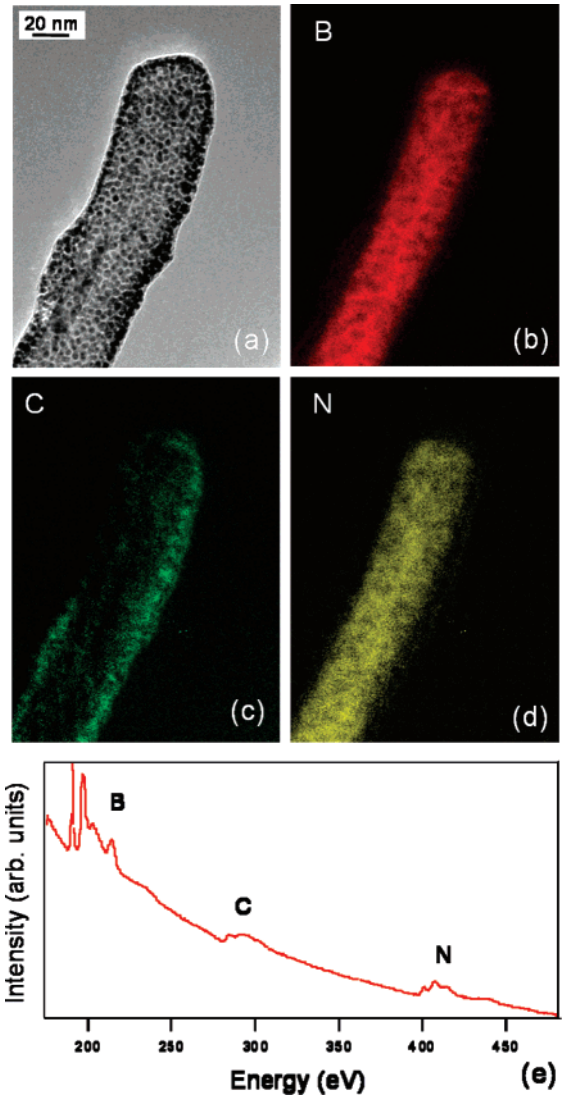

Figure 8. (a) Bright-field TEM image of DMAP−Au nanoparticles self-assembled at the surface of MPA-BNNTs, (b) elemental mapping of B present in part a, (c) elemental mapping of C present in part a, (d) elemental mapping of N present in part a, and (e) EEL spectrum of materials in part a.

gold nanoparticles. It is noted that this situation is rare and generally the BNNTs were coated in a monolayer of nanoparticles. High-resolution TEM (HR-TEM) was also used to image the structure of the nanoparticles assembled on the MPA-BNNTs (Figure 7). Also evident from the TEM analysis is the presence of an organic residue on the gold nanoparticles. This most likely involves the DMAP molecules that stabilize the nanoparticles and are free in the nanoparticle suspension. Because the thiol groups on the BNNTs have a higher affinity for the surface of the gold nanoparticles than the DMAP molecules, the presence of the molecules is not believed to hinder the assembly process.

Electron energy loss spectroscopy (EELS) was used as an additional means to characterize the assembly of the gold nanoparticles at the surface of the MPA-BNNTs, as shown in Figure 8. It can be seen from the bright-field image shown in Figure 8a that the diameter of the nanotube−nanoparticle assembly is approximately 57 nm. From the elemental mapping images of B and N, Figure 8b and d, respectively, the diameter of the structure attributed to the elements is estimated to be approximately 38 nm, whereas the diameter of the carbon elemental map in Figure 8c is approximately 57 nm (See the Supporting Information). This is consistent with the average diameter of the nanoparticles being 5 nm as measured by TEM while also allowing for the presence of both the organic layer at the surface of the nanotubes and the stabilizing ligands at the surface of the nanoparticles.

Figure 8e shows the EEL spectrum of the assembly and indicates the composition ratio of B and N in the structure to be nearly equal to 1, which confirms the stoichiometry of the BN nanotube. These results confirm that the BN nanotube is present in the center of the structure and also that the outer layer of nanoparticles and stabilizing ligands constitutes a layer approximately 5-nm-thick around the BNNT.

Control experiments were also conducted to support the assertion that the principal driving force for the self-assembly of the nanoparticles was strong and weak covalent bond formation in the case of the amine- and thiol-functionalized BNNTs, respectively. In one case, DMAP−Au nanoparticles were combined with a freshly sonicated suspension of as-produced BNNTs under conditions identical to that of the MPA-BNNTs. Following equilibration of the materials for 12 h, TEM analysis of the materials showed that there was negligible assembly of the gold nanoparticles at the surface of the BNNTs (Figure 9).

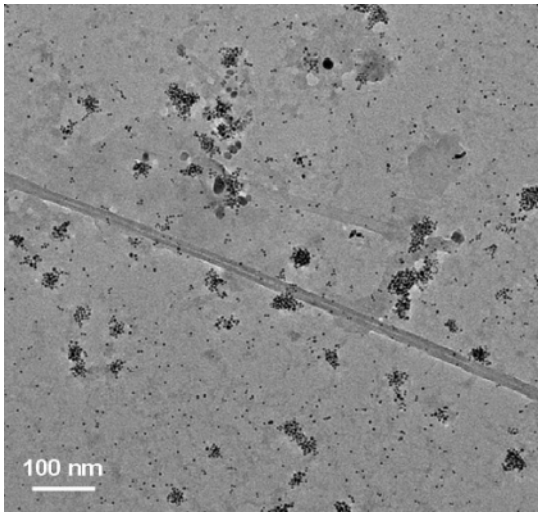

Figure 9. Control experiment, a low-resolution TEM image showing as-produced BNNTs following their combination with DMAP−Au nanoparticles.

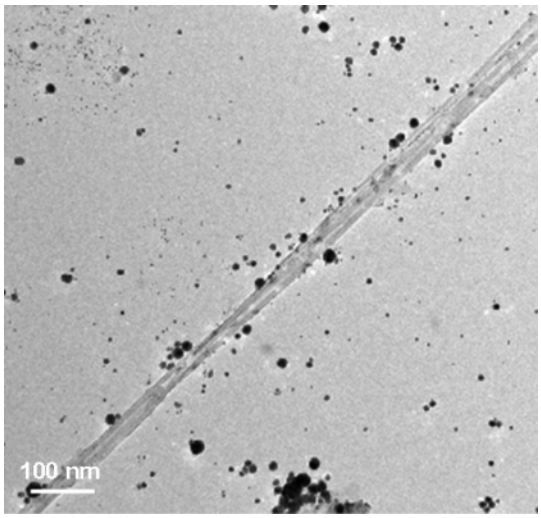

Figure 10. Control experiment, a low-resolution TEM image showing BC-modified BNNTs following their combination with DMAP−Au nanoparticles.

The lack of interaction between the as-produced BNNTs and the gold nanoparticles indicates that there is no strong intrinsic attractive force between the materials under these conditions. A second control experiment involved the combination of BNNTs that had been surface-modified with butyryl chloride (BC) molecules via amide formation (BC-modified BNNTs) with DMAP−Au nanoparticles. In this case, the coupling of short alkyl-chain molecules to the amine groups at the surface of the BNNTs is expected to both terminate the amine functionalities on the BNNTs and create a layer of organic molecules at the surface of the nanotubes similar to that of the MPA-BNNTs but without the thiol moieties. Following equilibration of the materials for 12 h, TEM analysis of the materials showed that there was negligible assembly of the gold nanoparticles at the surface of the BNNTs (Figure 10).

Both control experiments demonstrate a significant lack of interaction between the BNNTs and the DMAP−Au nanoparticles, where in one case the amine groups are absent at the surface of the nanotube and in another case where short-alkyl chains without thiol groups are present at the surface of the nanotubes. This also supports the assumption that the principal interaction between the amine- and thiol-functionalized BNNTs and the gold nanoparticles is covalent bond formation. In addition, in the case of both the amine- and thiol-functionalized BNNTs the dense coverage of gold nanoparticles is believed to be due to the significant functionalization of the surface of the BNNTs. The marked difference in the case of the control experiments indicates that the presence of functional groups at the surface of the BNNTs is the dominant factor that controls the self-assembly of the materials in solution.

To the best of our knowledge, this report is the first example of its kind to describe the functionalization of BNNTs with a high density of surface functional groups and to use these groups to immobilize gold nanoparticles in solution. We believe that the approach described in this report represents a significant result, whereby the amine modification of the BNNTs allows functional groups to be coupled with the surface of the BNNTs. This enables the functional groups to address other species in solution due to the length and flexibility of the organic chain that is extended from the surface. The use of a functional group such as a thiol means that these groups may be used to immobilize other materials such as Ag, Pd, CdS, CdSe, ZnS, and other materials that form bonds with thiols.

The use of both amine and thiol functional groups on the BNNTs means that materials can be immobilized at the surface of the BNNTs mediated by weak and strong covalent bond formation depending on the material used. This also means that the functional group at the surface of the BNNTs can be readily interchanged on account of the reactivity of groups such as amines and thiols. Such tuning of the interaction between nanoscale materials is of interest so that assembled materials can be further processed while immobilized or disassembled if necessary. It is therefore clear that such an approach has a great deal of versatility and that this extension of our previous result allows us to manipulate the chemical functionality at the surface of the BNNTs.

Conclusions

We have demonstrated the covalent modification of amine-functionalized BNNTs to form thiol-functionalized BNNTs. We have also demonstrated the self-assembly of gold nanoparticles at the surface of both amine- and thiol-functionalized BNNTs in aqueous solution via weak and strong covalent bond formation. The formation of such nanoscale assemblies is of interest in order to utilize the intrinsic properties of BNNTs or to use the BNNTs as nanoscale scaffolds for the assembly of technologically relevant materials. It is envisaged that such assemblies may form quasi one-dimensional nanoparticle networks that could be used for various applications such as single-electron transistors, biosensors, and plasmon waveguides or for the formation of novel composite and catalytic materials.[41−45]

Acknowledgment. This work was supported in part by the Director, Office of Energy Research, Office of Basic Energy Science, Division of Materials Sciences, Lawrence Berkeley National Laboratory under the U.S. Department of Energy, Contract No. DE-AC03-76SF00098 and by Defense Advanced Research Projects Agency (DARPA), Contract No. HR0011-04-1-0040. Portions of this work were performed at the Molecular Foundry, Lawrence Berkeley National Laboratory, which is supported by the Office of Science, Office of Basic Energy Sciences, of the U.S. Department of Energy under Contract No. DE-AC02-05CH11231.

Supporting Information Available: FT-IR spectrum of BC-modified BNNTs (Figure S1). TEM image of DMAP-stabilized

gold nanoparticles (Figure S2). UV−vis absorption spectra for DMAP-stabilized gold nanoparticles (Figure S3). Bright-field TEM image of BNNT−nanoparticle assembly with corresponding histogram (Figure S4). Elemental mapping images of BNNT−nanoparticle assembly for boron, carbon, and nitrogen with corresponding histograms (Figures S5, S6, and S7 respectively). This material is available free of charge via the Internet at http://pubs.acs.org.

References and Notes

(1) Liz-Marzan, Luis M. *Nanoscale Materials*; Kluwer Academic Publishers: Boston, MA, 2002.

(2) Dai, H. *Acc. Chem. Res*. **2002**, *35*, 1035.

(3) Zettl, A. *Adv. Mater*. **1996**, *8*, 443.

(4) Tasis, D.; Tagmatarchis, N.; Bianco, A.; Prato, M. *Chem. Rev*. **2006**, *106*, 1105.

(5) Kahn, M. G. C.; Banerjee, S.; Wong, S. S. *Nano Lett*. **2002**, *2*, 1215.

(6) Blake, R.; Gun'ko, Y. K.; Coleman, J.; Cadek, M.; Fonseca, A.; Nagy, J. B.; Blau, W. J. *J. Am. Chem. Soc*. **2004**, *126*, 10226.

(7) Gao, J.; Zhao, B.; Itkis, M. E.; Bekyarova, E.; Hu, H.; Kranek, V.; Yu, A.; Haddon, R. C. *J. Am. Chem. Soc*. **2006**, *128*, 7492.

(8) Jiang, K.; Schadler, L. S.; Siegel, R. W.; Zhang, X.; Zhang, H.; Terrones, M. *J. Mater. Chem*. **2004**, *14*, 37.

(9) Jung, M.-S.; Jung, S.-O.; Jung, D.-H.; Ko, Y. K.; Jin, Y. W.; Kim, J.; Jung, H.-T. *J. Phys. Chem. B* **2005**, *109*, 10584.

(10) Bekyarova, E.; Davis, M.; Burch, T.; Itkis, M. E.; Zhao, B.; Sunshine, S.; Haddon, R. C. *J. Phys. Chem. B* **2004**, *108*, 19717.

(11) Klinke, C.; Hannon, J. B.; Afzali, A.; Avouris, P. *Nano Lett*. **2006**, *6*, 906.

(12) Liao, S.; Holmes, K.-A.; Tsaprailis, H.; Birss, V. I. *J. Am. Chem. Soc*. **2006**, *128*, 3504.

(13) Wildgoose, G. G.; Banks, C. E.; Compton, R. G. *Small* **2006**, *2*, 182.

(14) Zhi, C.; Bando, Y.; Tang, C.; Xie, R.; Sekiguchi, T.; Golberg, D. *J. Am. Chem. Soc*. **2005**, *127*, 15996.

(15) Xie, S.-Y.; Wang, W.; Shiral Fernando, K. A.; Wang, X.; Lin, Y.; Sun, Y.-P. *Chem. Commun*. **2005**, 3670.

(16) Zhi, C.; Bando, Y.; Tang, C.; Honda, S.; Sato, K.; Kuwahara, H.; Golberg, D. *Angew. Chem., Int. Ed*. **2005**, *44*, 1.

(17) Tang, C.; Bando, Y.; Huang, Y.; Yue, S.; Gu, C.; Xu, F.; Golberg, D. *J. Am. Chem. Soc*. **2005**, *127*, 6552.

(18) Han, W.-Q.; Zettl, A. *J. Am. Chem. Soc*. **2003**, *125*, 2062.

(19) Zhi, C.; Bando, Y.; Tang, C.; Golberg, D. *J. Am. Chem. Soc*. **2005**, *127*, 17144.

(20) Zhi, C.; Bando, Y.; Tang, C.; Golberg, D. *J. Phys. Chem. B* **2006**, *110*, 8548.

(21) Fresco, Z. M.; Fréchet, J. M. J. *J. Am. Chem. Soc*. **2005**, *127*, 8302.

(22) Daniel, M.-C.; Astruc, D. *Chem. Rev*. **2004**, *104*, 293.

(23) Ikuno, T.; Sainsbury, T.; Okawa, D.; Fréchet, J. M. J.; Zettl, A. *Solid State Commun*. **2007**, *142*, 643.

(24) Tang, C.; Bando, Y.; Sato, T.; Kurashima, K. *Chem. Commun*. **2002**, 1290.

(25) Gittins, D. I.; Caruso, F. *Angew. Chem., Int. Ed*. **2001**, *40*, 3001.

(26) Chen, X.; Gao, X. P.; Zhang, H.; Zhou, Z.; Hu, W. K.; Pan, G. L.; Zhu, H. Y.; Yan, T. Y.; Song, D. Y. *J. Phys. Chem. B* **2001**, *109*, 11525.

(27) Kim, S. Y.; Park, J.; Choi, H. C.; Ahn, J. P.; Hou, J. Q.; Kang, H. S. *J. Am. Chem. Soc*. **2007**, *129*, 1705.

(28) Goto, T.; Hirai, T. *J. Mater. Sci. Lett*. **1988**, *7*, 548.

(29) Ramanathan, T.; Fisher, F. T.; Ruoff, R. S.; Brinson, L. C. *Chem. Mater*. **2005**, *17*, 1290.

(30) Sugino, T.; Tai, T.; Etou, Y. *Diamond Relat. Mater*. **2001**, *10*, 1375.

(31) Borowiak-Palen, E.; Pichler, T.; Fuentes, G. G.; Bendjemil, B.; Liu, X.; Graff, A.; Behr, G.; Kalenczuk, R. J.; Knupfer, M.; Fink, J. *Chem. Commun*. **2003**, 82.

(32) Zhi, C.; Bando, Y.; Tang, C.; Honda, S.; Sato, K.; Kuwahara, H.; Golberg, D. *J. Phys. Chem. B* **2006**, *110*, 1525.

(33) Huang, Q.; Bando, Y.; Zhi, C.; Golberg, D.; Kurashima, K.; Xu, F.; Gao, L. *Angew. Chem., Int. Ed*. **2006**, *45*, 2044.

(34) Pouchert, C. J. *The Aldrich Library of FT-IR Spectra*, 2nd ed.; Aldrich Chemical Co.: Milwaukee, WI, 1997.

(35) Leff, D. V.; Brandt, L.; Heath, J. R. *Langmuir* **1996**, *12*, 4723.

(36) Ou, Y. −Y.; Huang, M. H. *J. Phys. Chem. B* **2006**, *110*, 2031.

(37) Vossmeyer, T.; Jia, S.; DeIonno, E.; Diehl, M. R.; Kim, S. −H.; Peng, X.; Alivisatos, A. P.; Heath, J. R. *J. Appl. Phys*. **1998**, *84*, 3664.

(38) Sainsbury, T.; Stolarczyk, J.; Fitzmaurice, D. *J. Phys. Chem. B* **2005**, *109*, 16310.

(39) Zanella, R.; Basiuk, E. V.; Santiago, P.; Basiuk, V. A.; Mireles, E.; Puente-Lee, I.; Saniger, J. M. *J. Phys. Chem. B* **2005**, *109*, 16290.

(40) Azamian, B. R.; Coleman, K. S.; Davis, J. J.; Hanson, N.; Green, M. L. H. *Chem. Commun*. **2002**, *4*, 366.

(41) Simon, U. *Adv. Mater*. **1998**, *10*, 1487.

(42) Haes, A. J.; Duyne, R. P. V. *J. Am. Chem. Soc*. **2002**, *124*, 10596.

(43) Maier, S. A.; Kik, P. G.; Atwater, H. A.; Meltzer, S.; Harel, E.; Koel, B. E.; Requicha, A. A. G. *Nat. Mater*. **2003**, *2*, 229.

(44) Gao, J.; Zhao, B.; Itkis, M. E.; Bekyarova, E.; Hu, H.; Kranak, V.; Yu, A.; Haddon, R. C. *J. Am. Chem. Soc*. **2006**, *128*, 7492.

(45) Liao, S.; Holmes, K.-A.; Tsaprailis, H.; Birss, V. I. *J. Am. Chem. Soc*. **2006**, *128*, 3504.